Chapter 7

Preparation, characterization and gas sensing performance of Cr-doped SnO_2 (CTO) thin films

Publication:

- Ganesh E. Patil, D. D. Kajale, V. B. Gaikwad, N. K. Pawar and G. H. Jain, "Properties and Gas Sensing Mechanism Study of CTO Thin Films as Ethanol Sensor", *Sensors & Transducers Journal*, Vol. 137, Issue 2, February 2012, pp. 47-58.

Chapter 7

Preparation, characterization and gas sensing performance of Cr-doped SnO_2 (CTO) thin films

Figure captions

Table caption

7.0 Introduction

Hydrocarbon gases, widely used as industrial and domestic fuels, have often proved to be hazardous because of explosions caused by leaks. It is therefore of vital importance to develop good sensors for hydrocarbon gases. Metal oxide gas sensors are the most commercialized type of gas sensors. Semiconductor metal oxides, such as tin oxide, zinc oxide, titanium oxide, zirconium oxide, indium oxide, etc have long been investigated as sensing materials [1-7]. Unfortunately, such problems as poor selectivity and long term stability have not been solved throughout. An improvement of these properties requires a better understanding of the sensing mechanisms. Recent developments and current status of semiconducting gas sensors have been reviewed by some authors [8-13]. In this area, tin oxide (SnO_2) sensor material has been widely applied as a basic material in gas sensors primarily due to its high response and low cost [14]. In SnO_2 sensors, the gas sensing mechanism can be described in terms of an adsorption/desorption process of oxygen at the surface of a sensing element. Thus, for the complete description of sensor response, the interactions between the sensor element and the target gas should be clarified. The reaction mechanism of alcohol detection by tin oxide films was extensively investigated to understand the nature of alcohol gas detection. In particular, Ogawa et al. [15], Kohl [16] and Rao et al. [17] reported the interaction of ethanol vapor with a SnO_2 surface. However, generally recognized poor selectivity and low thermodynamic stability of SnO_2 at elevated temperatures have given rise to the search for new active materials. Additives, such as metal oxides, are known to improve the response and selectivity of SnO_2 sensors. The acidic Al_2O_3 and basic La_2O_3 additives are known to improve the response to CO and ethanol, respectively [18, 19]. Therefore, it is highly desired to synthesize nanostructured SnO_2 that have not only designed the crystal structure, shapes with high response but also selectivity, quick response and recovery. It is well known that the doping with proper element is widely used as an effective method to increase response with selective gas sensor materials.

Cr is an important transition metal element and it has close ionic radius parameter to that Sn^{4+}, which means that Cr^{3+} can easily penetrate into crystal lattice or substitute Sn^{4+}

position crystal. However, there are no reports in literature dealing with Cr doped tin oxide (CTO) ethanol sensors. Efforts have therefore been made to develop Cr doped tin oxide thin film gas sensors for the detection of ethanol vapors and for the improvement in its sensing performance of the thin films.

Spray pyrolysis technique (SPT) is useful alternative to the traditional methods for obtaining thin films. It is of particular interest because of its simplicity, low cost and minimal waste production. In this technique, a solution consisting of the ions of required compound is sprayed on a heated substrate and their pyrolysis results in deposition of the compound in thin film form. The chemical reactants are selected such that the products other than the desired compound are volatile at the temperature of deposition [20]. The aim of the present work is to develop the sensor with CTO thin film prepared by spray pyrolysis technique, which could be able to detect the ethanol vapors.

7.1 Experimental procedure

7.1.1 Preparation of CTO thin film

A 0.01M aqueous methanol solution of a mixture of chromium oxide (CrO_3, Sigma-Aldritch) and $SnCl_4.5H_2O$ (Sigma-Aldritch), Cr:Sn=1:9 mole ratio, was chosen as the precursor for the preparation of CTO thin films. The experimental set-up used for preparation of thin films is shown in chapter 3 (Fig. 3.1). Air was employed as the carrier gas, and the substrate temperature was 350 ^oC. The glass substrates were ultrasonically pre-treated in acetone and ethanol, followed by ultrasonic cleaning in distilled water prior to deposition. The solution was sprayed continuously through a glass nozzle of 0.1 mm inner diameter onto glass substrate. The deposition parameters like spray rate 5 ml/min. was adjusted using air as a carrier gas, nozzle to substrate distance (25 cm) were kept constant, and to and fro frequency of the nozzle (18 cycles min^{-1}) were kept constant at the optimized values indicated in brackets [21, 22].

7.1.2 Mechanism for formation of CTO thin films

The sprayed droplets undergo solvent evaporation, solute condensation and thermal decomposition, thereby resulting in the formation of thin films. 0.1% of chromium

dopant in the tin matrix was achieved using of Cr^{6+} containing oxide (CrO_3, 99.9%). In solution, Cr^{6+} reduces to Cr^{3+}, following the equations:

$$CrO_3 + H_2O \rightarrow H_2CrO_4 \quad (1)$$

or

$$2CrO_3 + H_2O \rightarrow H_2Cr_2O \quad (2)$$

The necessary water for hydrolysis was supplied from the solution itself, since the methanol solution contained 4% water. The obtained acids are unstable and reduce to Cr^{3+}, in alcohol solution:

$$2H_2CrO_4 \rightarrow Cr_2O_3 + 3/2O_2 + 2H_2O \quad (3)$$

$$H_2Cr_2O_7 \rightarrow Cr_2O_3 + 3/2O_2 + H_2O \quad (4)$$

The pyrolytic reaction takes place on a heated substrate, leading to a nano-crystalline metal oxide. The usual expression for this reaction is:

$$SnCl_4.5H_2O \xrightarrow{350\ ^oC} SnO_2 + 4HCl + 3H_2O \quad (5)$$

For the Cr-doped films, it can be written:

$$(1-x)SnO_2 + x/2Cr_2O_3 \rightarrow Cr_xSn_{1-x}O_{2-\delta} \quad (6)$$

where $Cr_xSn_{1-x}O_{2-\delta}$ is the chemical composition of the obtained films, with the atomic percentage of chromium: x = 0.1.

7.2 Characterization of CTO thin film

As prepared SnO_2 thin film was annealed at 550 ^oC for 30 min. The phase and crystallinity of CTO thin films were recorded on X-ray diffractometer using CuK_α radiation with a wavelength λ =1.5418 Å at 2θ values between 20^o and 80^o. The average crystallite size (D) was estimated using the Scherrer equation [23] as follows:

$$D = 0.9\ \lambda / \beta \cos\theta \quad (7)$$

where λ, β and θ are the X-ray wavelength, the full width at half maximum (FWHM) of the diffraction peak, and Braggs diffraction angle, respectively. A JEOL 2300 model (Japan) was used to examine the surface morphology of the sample by scanning electron microscopy (SEM) and the percentage of constituent elements was evaluated by the

energy dispersive analysis by X-rays (EDAX). Also surface morphology characterized by FESEM (HITACHI-S-4800 (II)). Gas response (S) is defined as the ratio of change in conductance of the sample on exposure to a test gas to the conductance in air [24, 25].

$$S = (Ia - Ig) / Ia = \Delta I / Ia \quad (8)$$

where Ig and Ia are the conductances of a sample in the presence and absence of a test gas, respectively, and ΔI the change in conductance. The sample was examined under different gases such as LPG, H_2, CO, CO_2, NH_3, O_2, Cl_2 and ethanol.

7.2.1 Structural properties of CTO thin films

7.2.1.1 X-ray diffraction (XRD) analysis

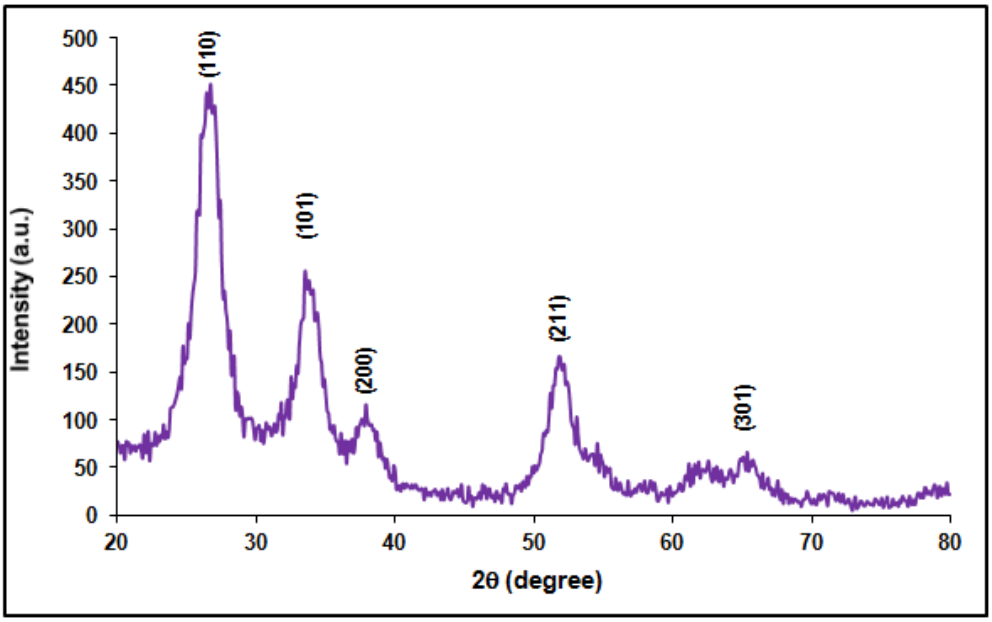

Fig. 7.1: X-ray diffraction pattern of CTO thin film.

The X-ray diffraction pattern of the CTO thin film is shown in Fig. 7.1. It shows well-defined broad diffraction peaks, indicating formation of polycrystalline phases. The diffraction peak indexing, done by matching with the Joint committee on powder diffraction standard (JCPDS) (no. 77-0452), clearly revealed formation of the SnO_2 phases with tetragonal structure. It was also seen that peaks corresponding to (110), (101), (200), (211) and (301) planes, with the (110) peak showing the highest intensity in

all peaks, implying that all the sample has a tetragonal crystal structure. No peaks belonging to Cr metal, Cr oxides or other impurity phases were detected within the response of our XRD measurements, indicating that the dopant was incorporated into the host lattice. The main peaks of Cr_2O_3 and CrO_3 phases should be present in the 28-32^o (2θ) range, where it is not observed any peak. Taking into account all these observations, one can conclude that the formation of tetragonal SnO_2 structure. These data indicate that Cr doping does not substantially alter the deposited crystal structure. As well known, the ionic radii of Cr^{3+} (0.62Å) is smaller than that of Sn^{4+} (0.69Å), therefore it is within expectation due to the substitutional incorporation of Cr dopant.The average crystallite size was determined using Scherrer equation which was observed to be 4 nm.

7.2.1.2 Scanning electron microscopy (SEM) and energy dispersive analysis by X-rays (EDAX)

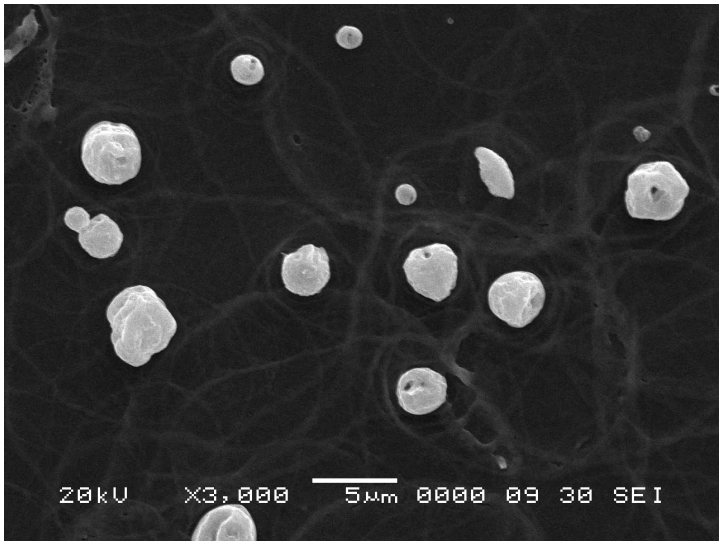

Fig. 7.2: SEM image of CTO thin film.

Fig. 7.2 shows SEM image of CTO thin film on glass substrate. It exhibit web-like surface morphology, covering the micropores on the surface. Chemical compositions of CTO thin film was investigated by energy dispersive analysis by X-ray (EDAX) as shown in Fig. 7.3. It indicates that thin film is composed of Sn, O and Cr, which is 29.82 at%, 60.75 at%, 9.43 at % respectively, demonstrating that the existence of chromium

within the sample. It implies that actual atomic percentage ratio of Cr is less than the nominal composition (10 at%) in the solution. The difference between the actual and the nominal Cr concentration is probably due to the dilution of Cr ions in the SnO_2 host matrix. It was found that the Cr doped SnO_2 thin film was tin deficient and oxygen rich, indicating that the Cr doped SnO_2 thin film was non-stoichiometric.

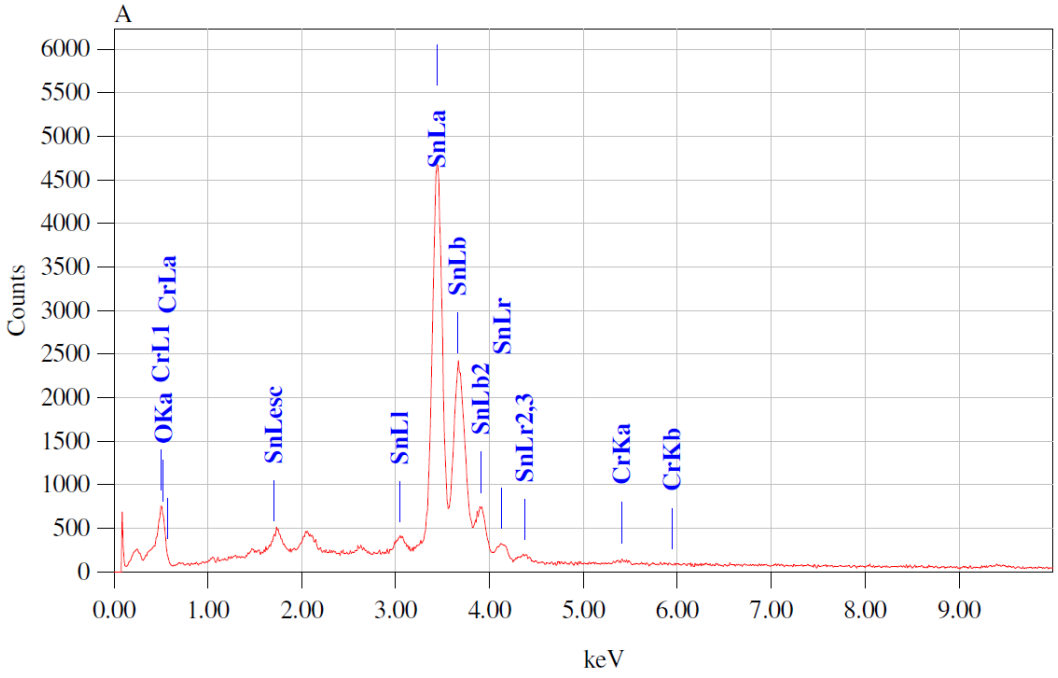

Fig. 7.3: EDAX spectra of CTO thin film.

7.2.1.3 FESEM analysis of CTO thin film

Surface morphological study of CTO thin film was carried out using field emission scanning electron microscopy. Fig. 7.4 shows FESEM images of CTO thin film with different magnification. Fig. 7.4 (a-d) shows the rare distribution of particles on surface with numerous minute pores with the ring type background pattern. Fig. 7.4 (e-h) showing the egg shell type structures with short ridges and very deep pores. Fig 7.4 (i, j) shows embryo type and skull type nature of particles formed on the surface.

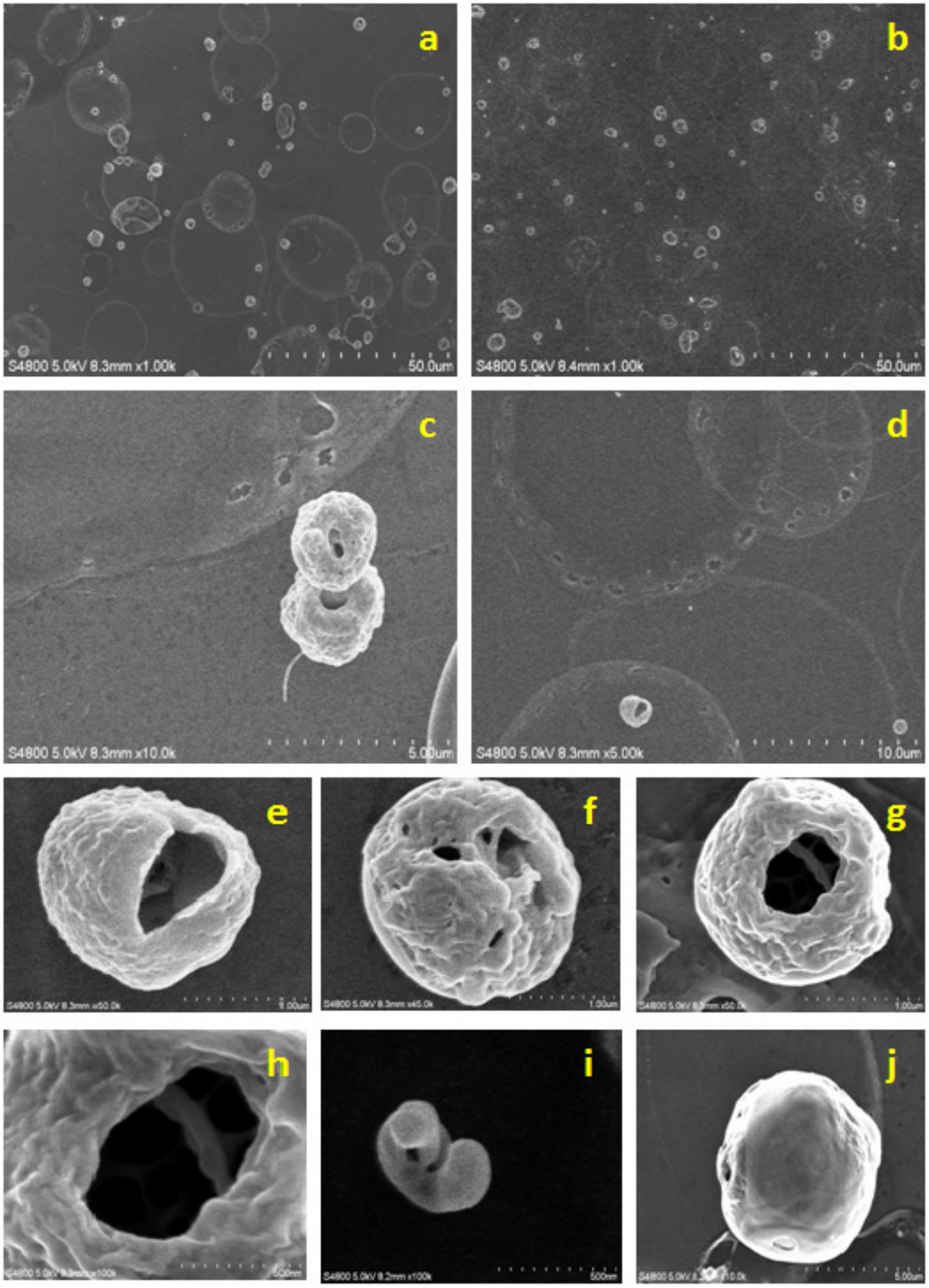

Fig. 7.4: FESEM images of CTO thin film at different spots (a, b) with high magnification (c, d) and different shapes of particles (e-j).

7.2.2 Optical properties of CTO thin film by UV-visible spectroscopy

The optical energy band gap of CTO thin film was estimated from optical absorption measurement. The optical absorption spectrum for the CTO thin film is recorded in the wavelength range of 300–600 nm at room temperature shown in Fig. 7.5.

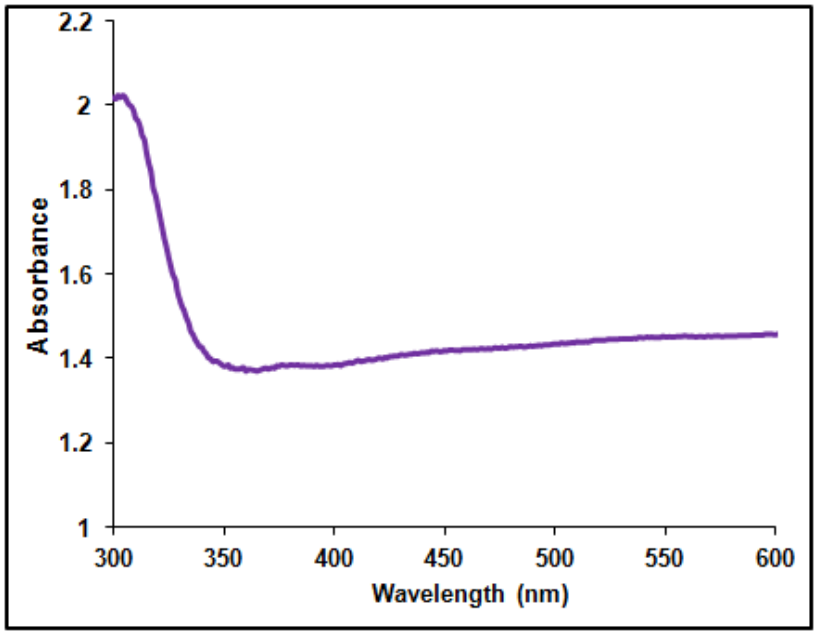

Fig. 7.5: UV-visible absorption spectra recorded for CTO thin film.

The optical absorption data were analyzed using the following classical relation of optical absorption in semiconductor near band edge [21]:

$$\alpha h\nu = A(h\nu - Eg)^n \qquad (9)$$

where α is absorption coefficient, A is constant, Eg is the separation between bottom of the conduction band and top of the valence band, $h\nu$ the photon energy and n is a constant. The value of n depends on the probability of transition; it takes values as 1/2, 3/2, 2 and 3 for direct allowed, direct forbidden, indirect allowed and indirect forbidden transition respectively. Thus, if plot of $(\alpha h\nu)^2$ versus $(h\nu)$ is linear the transition is direct allowed. Extrapolation, of the straight-line portion to zero absorption coefficient ($\alpha = 0$), leads to estimation of band gap energy (Eg) values. Fig. 7.6 shows variation of $(\alpha h\nu)^2$ as a function of photon energy $(h\nu)$. The band gap energy, calculated from the spectrum for film is 3.54 eV.

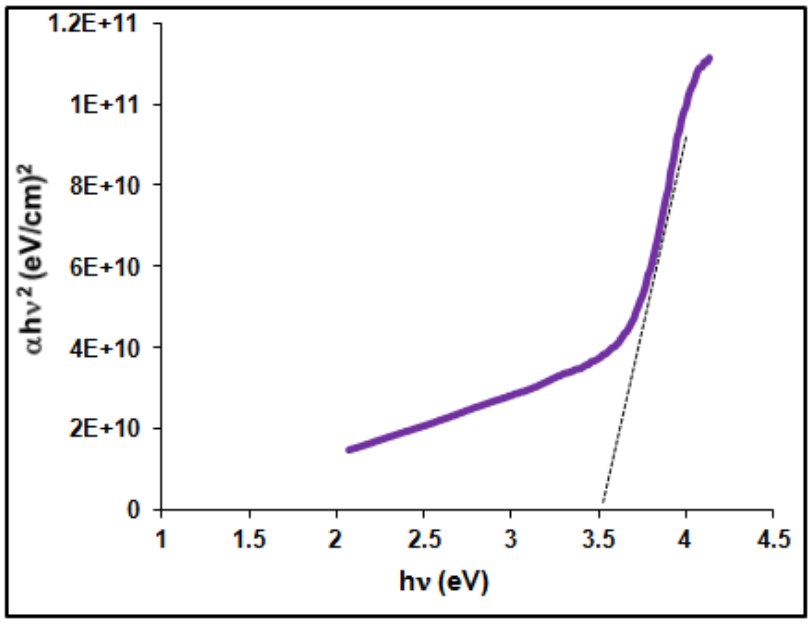

Fig. 7.6: Plot of the $(\alpha h\nu)^2$ verses photon energy ($h\nu$) for CTO thin film.

7.2.3 Electrical properties of CTO thin film sensor

7.2.3.1 I-V characteristics of CTO thin film

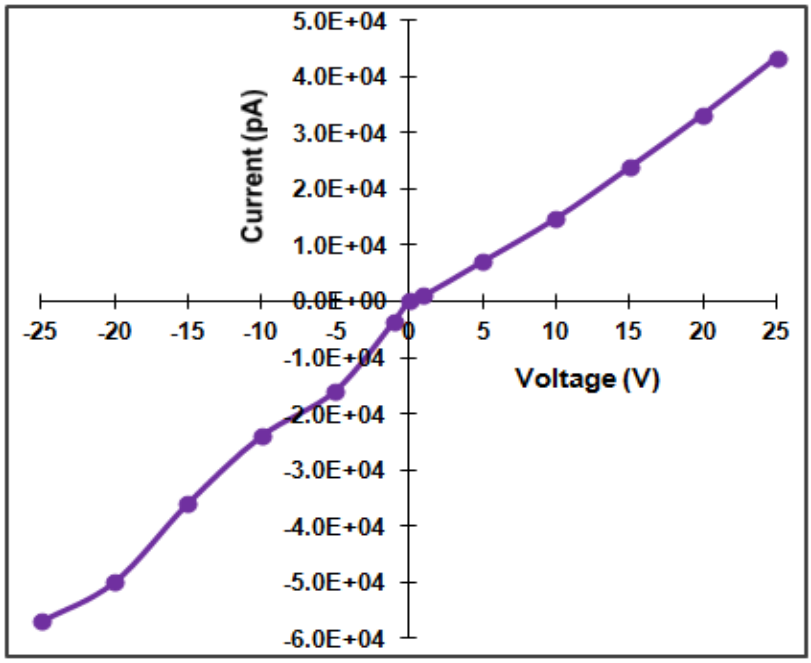

Fig. 7.7: I-V characteristics of CTO thin film.

Fig. 7.7 shows the I-V characteristics of CTO thin film, measured at room temperature and exhibited a linear dependence between current and voltage. Silver paste was used as a contacting electrode. This indicated an ohmic in nature of the silver contacts. Such linearity might arise due to essentially degenerately doped (high carrier concentration) SnO_2, where the tunnelling barrier becomes small and a quasi-ohmic contact is observed [26].

7.2.3.2 Electrical conductivity

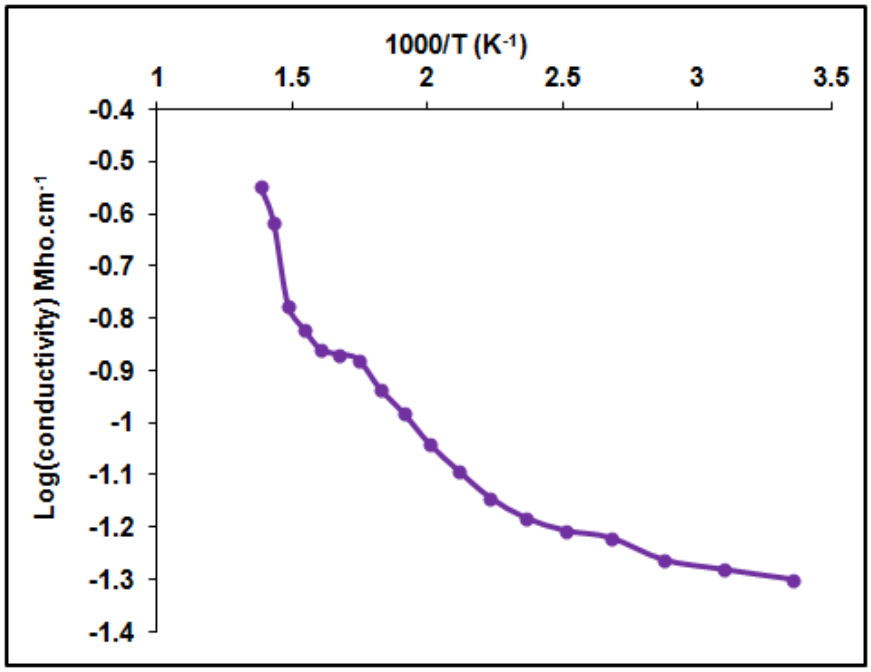

Fig. 7.8: Variation of conductivity with temperature.

Fig. 7.8 represents the variation of log (conductivity) verses temperature of CTO thin film. It is clear from the graph that the conductivity is varying with temperature. The addition of a trivalent cation such as Cr^{3+} to SnO_2 increases the number of oxygen vacancies. This causes an increase in the conductivity of the film according to the following mechanism.

$$2Cr^{3+} \rightarrow 2Cr'_{Sn} + V_o'' \qquad (10)$$

Where Cr'_{Sn} denotes a Cr occupying a Sn position, generating a negative charge.

7.2.3.3 Thermoelectric power (TEP) measurements

The thermoelectric power (TEP) was measured as a function of temperature in the range between 300 and 425 K. TEP is the ratio of thermally generated voltage to the temperature difference across the semiconductor. Diffusion of thermally generated majority charge carriers occurs from high temperature to the low temperature end, as a result of temperature difference (ΔT). This creates a positive space charge near high temperature end, which sets up an electric field or potential difference thereby giving rise to a thermal emf (ΔE). For SnO_2 material, conduction electrons originate from ionized defects such as oxygen vacancies, rendering n-type conductivity. The variation of the thermo emf with temperature difference (ΔT) for CTO thin film is shown in Fig. 7.9.

The rate of increment in TEP is higher in the range of ΔT from 355 to 375 K and thereafter slowed down. Initial increment is attributed to the increase in mobility of charge carriers and carrier concentration with rise in ΔT. The magnitude of TEP increases with rise in temperature difference (ΔT). The value of TEP lies in the range of 82–118 μVK^{-1}.

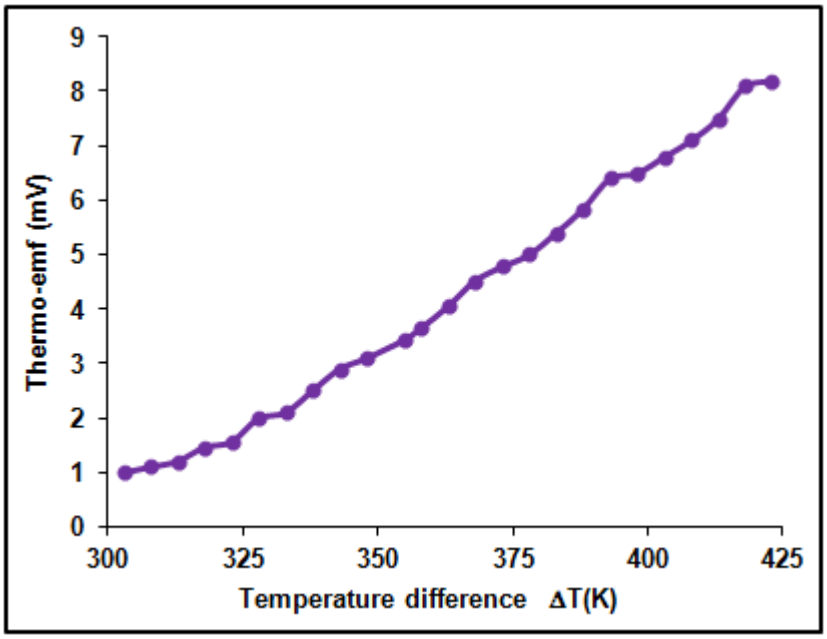

Fig. 7.9: Variation of the thermo emf with temperature difference (ΔT).

7.3 Gas sensing properties of CTO thin film

7.3.1 Principle of ethanol sensing mechanism

The mechanism of the ethanol detection by CTO thin film can be described as follows: At first oxygen is adsorbed on the oxide layer when the sensitive film is heated at ambient at a temperature of 50 ^{o}C –550 ^{o}C. The adsorption of the oxygen forms ionic species such as O^{2-}, O_2^- and O^-. These oxygen species when desorbed (desorption of O^2, O_2^- and O^- take place at 50 ^{o}C, 100 ^{o}C and 550 ^{o}C, respectively), result in the increase or decrease of the conductance of thin film layer depending on the nature of gas. Its conductivity increases when the incoming gas is reducing type and decreases when it is oxidizing type. At the higher temperature range only O^- species will react with the contaminant gas. The reaction kinematics will proceed like this:

$$O_{2\ (gas)} \leftrightarrow O_{2\ (ads)} \tag{11}$$

$$O_{2\ (ads)} + e^- \leftrightarrow O_{2\ (ads)}^- \tag{12}$$

$$O_{2\ (ads)} + e^- \leftrightarrow 2O_{(ads)}^- \tag{13}$$

The reaction between ethanol and ionic oxygen species takes place by two different ways:

$$C_2H_5OH_{\ (gas)} + O \leftrightarrow CH_3CHO + H_2O + e^- \tag{14}$$

$$C_2H_5OH_{\ (gas)} \leftrightarrow H + C_2H_5O_{\ (surface)} \tag{15}$$

$$C_2H_5OH \leftrightarrow H + CH_3CHO \tag{16}$$

$$CH_3CHO + O_{\ (bulk)} \leftrightarrow CH_3COOH + O_{\ (vacancies)} \tag{17}$$

7.3.2 Variation of response to ethanol with operating temperature

Fig. 7.10 shows the variation of gas response of CTO thin film sensor to 1000 ppm ethanol vapors with operating temperature. It is seen that for temperatures lower and higher than 300 ^{o}C, the response is less indicating 300 ^{o}C to be an optimum temperature. The highest response was obtained at 300 ^{o}C. It is reported that the highly active O^- is the dominant species in case of SnO_2 for temperature between 150 ^{o}C and 450 ^{o}C. The major adsorbed species in our films is therefore likely to be O^-. This adsorbed oxygen creates a

space charge region near the film surface by extracting electrons from the material. Ethanol, being reducing in nature, removes adsorbed O^- species from the surface and re-injects the electrons back to the material, thereby reducing the resistance, which resulted in higher response.

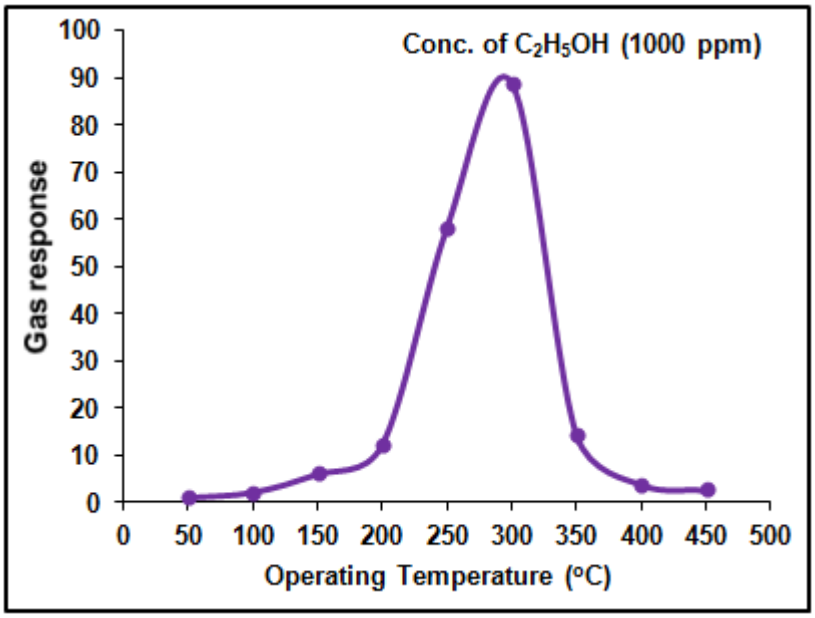

Fig. 7.10: Variation of response to ethanol with operating temperature.

7.3.3 Gas response with ethanol concentration

The dependence of the CTO thin film sensor's response on the concentrations of ethanol (10–1000 ppm) was investigated at 300 ^oC, and the result is shown in Fig. 7.11. As shown in the image, the CTO thin film sensors had good response to the ethanol even at low concentration of 10 ppm. Meanwhile, with increasing concentration of the ethanol, the response of the sensor sharply increased up to 1000 ppm. The rate increase of response was relatively larger up to 1000 ppm, smaller during 1000-1200 ppm and then saturates after 1000 ppm. Thus the active region of the sensor would be between 10-1000 ppm. At lower ethanol concentration, the monolayer of ethanol molecules would be expected to be formed on the surface which would interact with the surface more actively giving larger responses [27]. There would be multilayer of ethanol molecules on the sensor surface at the higher concentration resulting in saturation in response.

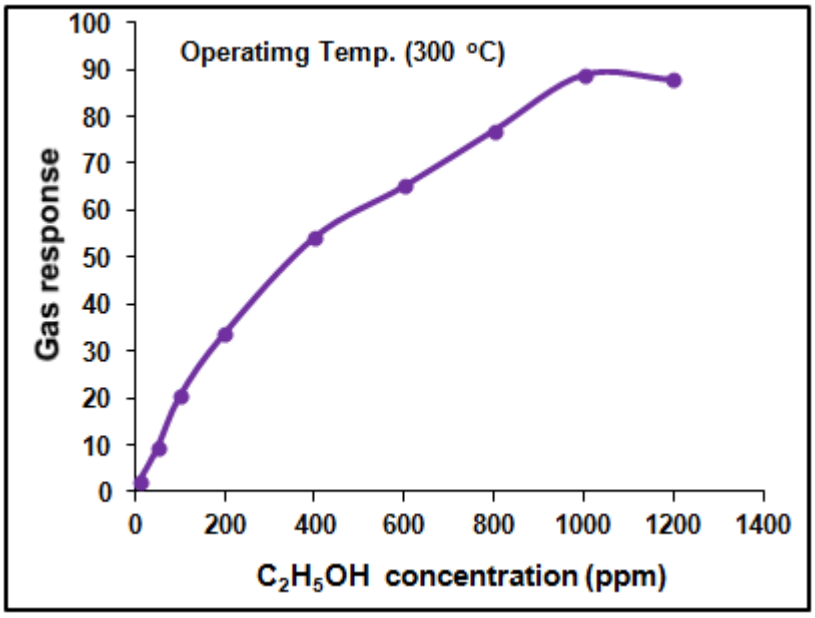

Fig. 7.11: Response with ethanol concentration at 300 ^{o}C.

7.3.4 Selectivity of CTO thin film against different gases

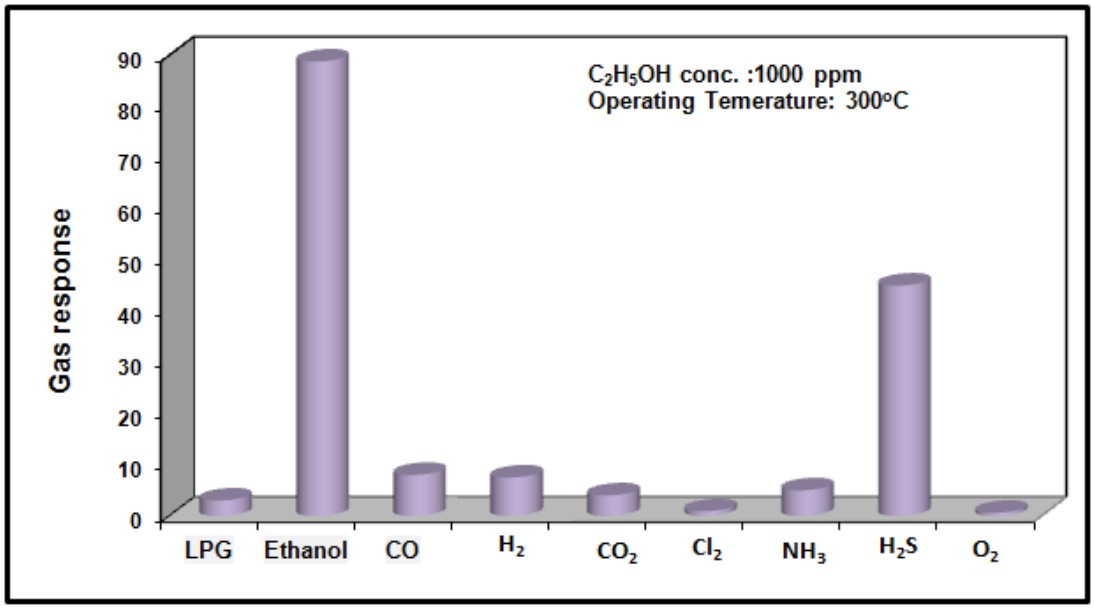

Fig. 7.12: Selectivity of film for various gases.

Besides ethanol, the sensing performances of the sensor to some other gases were also examined to depict its selectivity. Selectivity can be defined as the ability of a sensor to

respond to a certain gas in the presence of different gases [21]. Percent selectivity [24] of one gas over others is defined as the ratio of the maximum response of target gas (e.g. ethanol) to the maximum response of other gas at optimum temperature of target gas,

$$\% \text{ Selectivity} = (S_{\text{other gas}} / S_{\text{Target gas}}) \times 100 \qquad (18)$$

Fig. 7.12 depicts the gas response of thin film sensor for ethanol (1000 ppm) against other tested gases at 300 ^{o}C. The film showed the high response for ethanol among the following gases: LPG, NH_3, CO, CO_2, H_2, H_2S, O_2 and Cl_2. Table 7.1 shows the gas response and corresponding selectivity of gases against ethanol at 300 ^{o}C. The selectivity of ethanol is considered as 100 %.

It is observed from Table 7.1 and Fig. 7.12 that CTO thin film has more response to ethanol and it has relatively high selectivity against other gases. This is the main feature of pure CTO thin film sensor.

Table 7.1: Gas response and selectivity of CTO thin film for different gases at 300^{o}C operating temperature.

Gas	Gas response	Selectivity in %
LPG	3	3.37
Ethanol	88.8	100
CO	8	9.0
H_2	7.5	8.44
CO_2	4	4.50
Cl_2	0.9	1.0
NH_3	5	5.63
H_2S	45	50.67
O_2	0.6	0.67

7.3.5 Response and recovery time

The response time and recovery time (defined as the time required to reach 90% of the final equilibrium value) are represented in Fig. 7.13. The response was quick (~8 s) while the recovery was fast (~36 s). The quick response may be due to faster oxidation of gas. The negligible quantity of the surface reaction product and its high volatility explains

its quick response and fast recovery to its initial chemical status. Such a result indicates the good response speed of the sensors fabricated here.

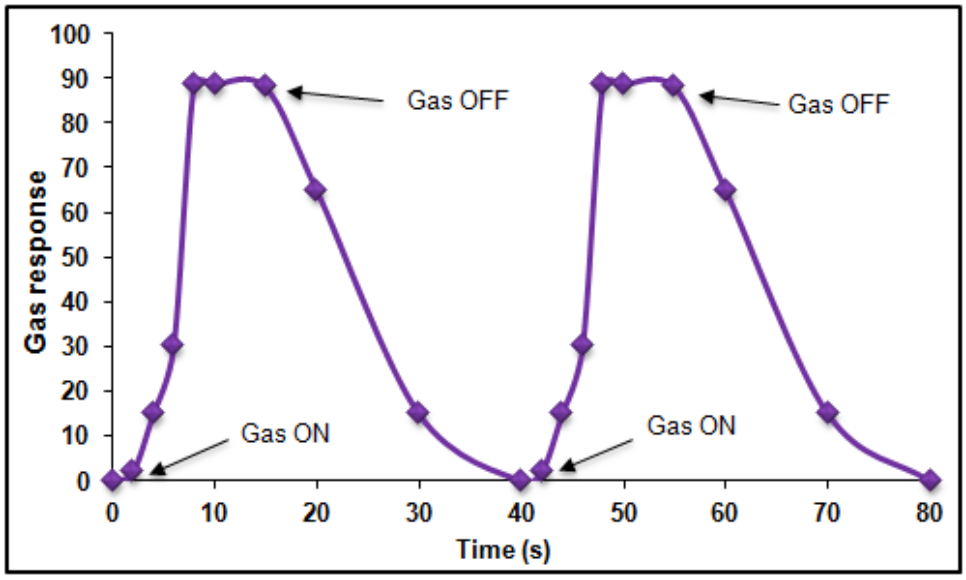

Fig. 7.13: Response and recovery time of CTO thin film sensor.

7.4 Conclusions

Based on the XRD, SEM, FESEM, optical absorption and gas sensing properties of CTO thin film prepared by spray pyrolysis technique (SPT) the following main points emerges:

i) Thin film showed the tetragonal structure with a strong (110) preferred orientation. Cr incorporation did not significantly change the crystal structure of SnO_2. The average crystallite size was 4 nm.

ii) SEM and FESEM analysis shows the rare distribution of particles on surface with numerous minute pores with the ring type background pattern containing nanoparticles on the surface of thin film.

iii) From TEP study, it shows the CTO thin film has n-type conductivity.

iv) Band gap obtained from UV- spectra is 3.54 eV.

v) CTO thin film was observed to be more sensitive to ethanol than the responses to other gases. The sensor has good selectivity to ethanol against LPG, CO_2, NH_3, C_2H_5OH and Cl_2.

vi) The sensor showed quick response (8 s) and fast recovery (36 s).

vii) The results demonstrate that CTO thin films have excellent potential applications for fabrication high performance ethanol sensors.

References

[1]. G. Korotcenkov, I. Boris, V. Brinzari, Yu. Luchkovsky, G. Karkotsky, V. Golovanov, A. Cornet, E. Rossinyol, J. Rodriguez, A. Cirera, *Sens. Actuators B* **103 (**2004) 13.

[2]. N. Barsan and U. Weimar, *J.Phys. Condens. Matter* **15** (2003) R1.

[3]. N. Yamazoe, *Sens. Actuators B* **5** (1991) 7.

[4]. U. Kirner, K. D. Schierbaum, W. Gopel, B. Leibold, N. Nicoloso, W. Weppner, D. Fischer and W.F. Chu., *Sens. Actuators B* **1** (1990) 103.

[5]. G. N. Advani and L. Nanis, *Sens. Actuators B* **2** (1982) 201.

[6]. T. W. Capehart and S. C. Chang, *The J. Vac. Sci. Technol.* **18** (1981) 393.

[7]. Y. Liu, E. Koep and M. Liu, *Chem. Mater.l* **17** (2005) 3997.

[8]. S. Phadungdhitidhada, S. Thanasanvorakun, P. Mangkorntong, S. Choopun, N. Mangkorntong, D. Wongratanaphisan, *Curr. Appl. Phys.* **11** (2011) 1368.

[9]. H. Li, J. Xu, Y. Zhu, X. Chen and Q. Xiang, *Talanta* **82** (2010) 458.

[10]. I. S. Hwang, J. K. Choi, S. J. Kim, K.Y. Dong, J. H. Kwon, B. K. Ju, J. H. Lee, *Sens. Actuators B* **142** (2009) 105.

[11]. N. V. Hieu, *Sens. Actuators B* **144** (2010) 425.

[12]. J. Zhang, S. Wang, Y. Wang, M. Xu, H. Xia, S. Zhang, W. Huang, X. Guo and S. Wu, *Sens. Actuators B* **139** (2009) 369.

[13]. L. Xi, D. Qian, X. Tang and C. Chen, *Mater. Chem. Phys.* **108** (2008) 232.

[14]. D. Kohl, *Sens. Actuators B* **18 (**1989) 71.

[15]. H. Ogawa, M. Nishikawa, and A. Abe, *J. App. Phys*. **53** (1982) 4448.

[16]. D. Kohl, *J. Phys. D Appl. Phys.* **34** (2001) R125.

[17]. C. N. R. Rao, A. R. Raju and K. Vijayamohanan, *New Materials* Narosa Publishing House, New Delhi, India, (1992) 1.

[18]. K. Fukui and S. Nishida, *Sens. Actuators B* **45** (1997) 101.

[19]. Hae Won Cheong, Hee Sook Park Kim, Ki Hyun Yoon, *Key Engi. Mater.* **277** (2005) 403.

[20]. P. S. Patil, *Mater.Chem.Phys.* **59** (1999) 185.

[21]. G. E. Patil, D. D. Kajale, P. T. Ahire, D. N. Chavan, N. K. Pawar, S. D. Shinde, V. B. Gaikwad and G. H. Jain, *Bull. Mater. Sci.* **34 (**2011) 1.

[22]. G. E. Patil, D. D. Kajale, D. N. Chavan, N. K. Pawar, V. B. Gaikwad, G. H. Jain, *Sens. Trans. J.* **120 (**2010) 70.

[23]. B. D. Cullity, *Elements of X-ray diffraction,* USA: Addison-Wesley Publishing Co., (1956).

[24]. G. H. Jain, S. B. Nahire, Ganesh E. Patil, D. D. Kajale, S. D. Shinde, D. N. Chavan and V. B. Gaikwad, *New Developments and Applications in Sensing Technology, Lecture Notes in Electrical Engineering*, **83** (2011) 157.

[25]. S. D. Shinde, G. E. Patil, D. D. Kajale, V. B. Gaikwad and G. H. Jain, *Int. J. Nanoparticles* **5** (2012) 126.

[26]. S. M. Sze, *Semiconductor Devices, Physics and Technology*, New York: Wiley (1985) 169.

[27]. Hae-Won Cheong and Man-Jong Lee, *J.Ceram. Proc. Res.* **7** (2006) 183.

***